

# Mathematical modeling and experimental investigation of pressure characteristics inside the pilot stage of the deflector jet servo valve considering secondary jet velocity distribution

Proc IMechE Part G:  
J Aerospace Engineering  
2024, Vol. 238(16) 1624–1637  
© IMechE 2024  
Article reuse guidelines:  
[sagepub.com/journals-permissions](https://sagepub.com/journals-permissions)  
DOI: 10.1177/09544100241277234  
[journals.sagepub.com/home/pig](https://journals.sagepub.com/home/pig)  


Shenghong Ge<sup>1,2</sup> , Hanhao Yang<sup>1,2</sup> , Wenhao Cheng<sup>1</sup> and Yuchuan Zhu<sup>1</sup> 

## Abstract

Existing mathematical models for deflector jet hydraulic amplifiers cannot accurately describe the influence of the deflector motion on the receiver jet, which results in calculation differences for the receiver pressure. To deeply investigate this problem, the momentum transfer model considering secondary jet velocity distribution was used to develop an improved model that is more aligned with the actual state of the flow field. In this model, the receiver jet velocity is calculated, for the first time, with a maximum error of 18% when compared with existing models. To verify the improved model, the recovery pressures in the receivers were verified by numerical simulations and experiments. The verification results show that the model can accurately predict the recovery pressures in the receivers within an 8.1% maximum error. This model fills the gaps in the theoretical research and lays a foundation for the structural design of deflector jet pressure servo valves.

## Keywords

Deflector jet hydraulic amplifier, deflector jet pressure servo valve, receiver jet, numerical simulation, pressure characteristic

Date received: 18 July 2022; accepted: 29 July 2024

## Introduction

Aircraft anti-skid braking systems are important aircraft airborne devices that are vital participants in taking off and safe landing. A pressure servo valve is a core control element of an aircraft's anti-skid braking system, and the biggest advantage a deflector jet pressure servo valve has over a jet pipe pressure servo valve is a faster dynamic response. The moment of inertia of a deflector is smaller than that of a jet pipe. Hence, deflector jet pressure servo valves are highly reliable, have long service lives and a good dynamic performance, and they have extremely broad application prospects for mainstream military aircraft.<sup>1–4</sup>

To predict and control the performance of a servo valve, it is important to analyze the energy transfer process and flow field structure in the valve. However, the flow field in a deflector jet hydraulic amplifier, which is the pilot control stage in a deflector jet pressure servo valve, is very complex. Neither experimentation nor flow field numerical simulation can conveniently analyze and optimize the performance of a deflector jet hydraulic

amplifier. Therefore, a precise mathematical model is needed for the pilot stage in a deflector jet pressure servo valve.

Because of the similarities between the two, it is generally accepted that research regarding deflector jet hydraulic amplifiers is derived from research into jet pipe hydraulic amplifiers. Somashekhar<sup>5,6</sup> developed a jet pipe valve model based on throttling theory. Yin<sup>7,8</sup> developed a jet pipe valve mathematical model based on the Bernoulli equation. Hazem K. Abdallah<sup>9</sup> et al. used the LES

<sup>1</sup> College of Mechanical & Electrical Engineering, Nanjing University of Aeronautics and Astronautics, Nanjing, China

<sup>2</sup> Nanjing Mechatronics and Hydraulic Engineering Research Centre and Aviation Key Laboratory of Science and Technology on Aero Electro-mechanical System Integration, AVIC Nanjing Servo Control System Co. Ltd, Nanjing, China

## Corresponding author:

Yuchuan Zhu, College of Mechanical & Electrical Engineering, Nanjing University of Aeronautics and Astronautics, 29 Yudao St, Nanjing, China.

Email: [meeyczhu@nuaa.edu.cn](mailto:meeyczhu@nuaa.edu.cn)

method to analyze the influence of the geometric parameters of the jet outlet, amplifier and receiver on the flow field distribution characteristics of the front stage. Saha<sup>10</sup> carried out experimental and numerical studies on the flow field and cavitation phenomenon of the deflector jet servo valve in the pilot stage under different gas supply pressures. Li<sup>11</sup> et al. established a pressure-flow characteristic model of pre-jet amplifier based on turbulent jet theory, momentum conservation law and orifice throttling model, and obtained the pre-stage pressure gain coefficient through linearization of the theoretical model. The accuracy of the pressure gain coefficient is verified by simulation and experiment. Xing<sup>12</sup> et al. deduced the pressure characteristic model of the pre-jet amplifier based on Bernoulli equation and momentum theorem, and analyzed the application scope of the theoretical model. Furthermore, Zhu and Li<sup>13,14</sup> developed two static characteristic models, one based on the orifice flow formula and the other based on momentum theory, then compared the differences between the models. Moreover, the influence of structural parameters was also analyzed by assuming that the collision between the liquid and the jet can be approximated as the jet impact on a moving piston.<sup>15,16</sup>

By comparison, the hydraulic amplifier of a deflector jet valve is more complex than a jet pipe hydraulic amplifier because of its two jet stages, as opposed to the one in a jet pipe valve. Scholars have conducted many studies regarding the first jet stage.<sup>17–19</sup> As a result, current mathematical models can accurately describe the velocity distribution inside the deflector groove. However, studies regarding the second jet stage are still limited and primarily refer to the theoretical model for jet pipe hydraulic amplifiers. Kang<sup>18</sup> developed a fluidic resistor network model based on the outflow equation for the orifice. Furthermore, Yan<sup>18,19</sup> analyzed the pressure distribution using numerical simulation, then proposed an empirical formula. Saha<sup>20</sup> et al. considered two different flow states of laminar flow and turbulent flow respectively, and the mathematical model of pressure characteristics of deflecting jet amplifier was established based on the theory of wall-attached jet and momentum theorem. Mao<sup>21</sup> et al. proposed a theoretical model of the receiver based on the jet reflection hypothesis based on the momentum analysis of the jet acting on the receiver, and the expressions of the pressure and pressure gain of the left and right receivers are given. The experimental results show that the theoretical model can simulate the pressure characteristics of the pre-stage under the small deflection plate displacement. Aiming at the problem of zero offset caused by the asymmetric structure of the pre-amplifier of the deflection plate servo valve, Zhang<sup>22</sup> et al. analyzed the influence of the inconsistency of the fillet, inner angle and throat width of the two receiving chambers and the offset of the wedge relative to the jet port on the pressure characteristics and zero offset displacement of the amplifier. In these jet models, the momentum transfer model was widely used for modeling for the pilot stages of jet servo valves because it can reflect the physical mechanism involved in the

jet process. However, the existing momentum transfer models cannot describe the influence of the deflector motion on the jet velocities that impinge on the receiving chambers, which would result in a difference in the receiver pressure calculations.<sup>23,24</sup>

To improve the accuracy of the pilot stage model for deflector jet pressure servo valves, an improved model that is based on the momentum transfer model considering secondary jet velocity distribution and is more aligned with the actual flow field state was established. In this model, the receiver jet velocity is calculated, for the first time, to describe the effect of the deflector motion on the receiver jet flow field. To attain a better description of the internal flow characteristics of the deflector jet valve, a 3D numerical model with a high quality mesh was built. Finally, an experiment regarding the receiver pressure was performed to verify the theoretical and simulated analyses.

### Structure and principle

The structure of a deflector jet pressure servo valve is shown in [Figure 1](#).

The working principle of a deflector jet pressure servo valve, as shown in [Figure 1](#), is described next.

At null (no signal to the actuator), the deflector is in the middle of the jet pan and the jet stream impinges equally on the two receivers; therefore equal pressure is applied at each spool end. Because of the non-symmetrical structure of the spool, the second-stage spool remains at the left position. Therefore, the output pressure is equal to the return pressure.

When an electrical input signal is applied to the coils of the torque motor, an electromagnetic force is created. This force causes the deflector to move toward one of the two receivers, resulting in more fluid impinging on one receiving chamber than on the other, which causes the pressure at this receiver to be greater than at the other. The resulting differential pressure between the end chambers of the spool triggers spool motion.

The spool motion contributes to increases in the output pressure. The feedback chamber is connected to the output chamber by a pipeline inside the valve. Hence, the feedback pressure drives the spool to move in the opposite direction. Finally, there is a dynamic force balance between the left receiver pressure, the right receiver pressure, and the feedback pressure. As a result, the deflector jet pressure servo valve outputs a braking pressure proportional to the electrical input signal.

### Modeling of a deflector jet hydraulic amplifier

To obtain a clearer understanding of the jet flow process, the deflector jet flow field was divided into a first jet stage and a second jet stage, as shown in [Figure 2](#). In the first jet stage region, the hydraulic oil flowing from the inlet completes the first jet at the rectangular port of the jet pan, then collides with the sidewall of the deflector. In the second jet stage region, after the jet collides with the

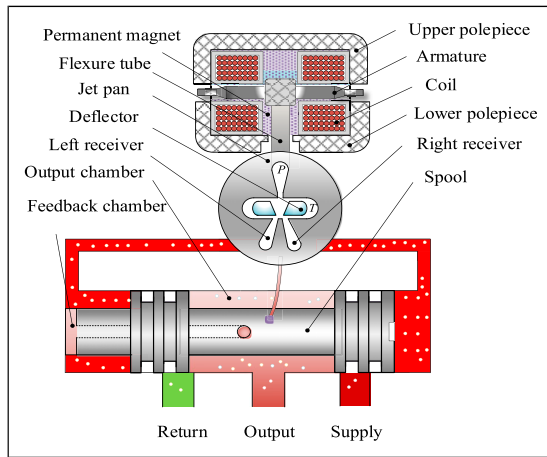


**Figure 1.** The structure of a deflector jet pressure servo valve.

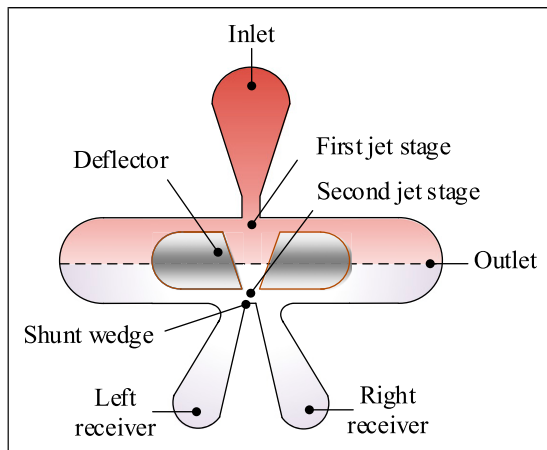


**Figure 2.** Flow field division of a deflector jet amplifier.

deflector, part of the oil flows downward to form a second jet. Then the second jet impinges on both the left and right receivers under the action of the shunt wedge.

According to the introduction, current mathematical models for the first jet stage can accurately describe the velocity distribution. Therefore, only the second jet stage was modeled during this study. This paper primarily proposes an improved model to obtain a better description of the effect of the deflector motion on the jet velocities that impinge on the receivers.

### Flow area model for the left and right receivers

As shown in Figure 3, the second jet impinges on the left and right receivers under the action of the shunt wedge. According to the momentum transfer model, the collision between the liquid and the jet can be considered as impact on a moving piston.<sup>15</sup> Therefore, the flow area model for the left and right receivers must be discussed in this way, and it directly affects the momentum of the moving piston. Moreover, the influence of the second jet expansion on the flow area must be considered as well.

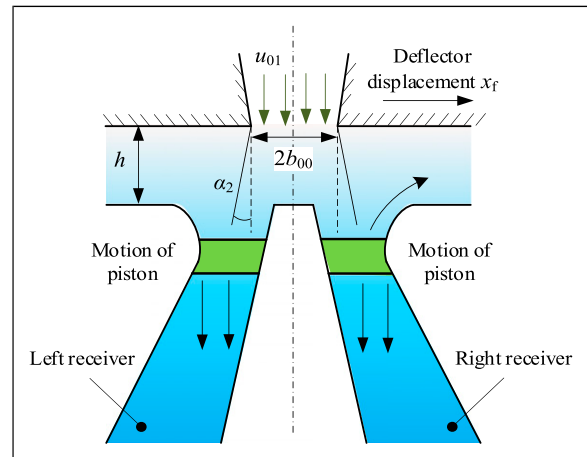


**Figure 3.** The second jet impinges on the left and right receivers.

As shown in Figure 4, the flow areas of the second jet covering the right and left receivers are denoted as  $A_{e1}$  and  $A_{e2}$ , respectively. Similarly, the flow areas not covering the right and left receivers are represented by  $A_{e3}$  and  $A_{e4}$ , respectively.

It was assumed that  $x_f$  is the displacement of the deflector and that the relative distance between the deflector and the receivers is given by  $\lambda_j = h/(2b_{00})$ . If the jet type coefficient,<sup>15</sup> which represents the momentum loss during the jet process, is  $\psi$  ( $0 < \psi < 1$ ), and if the expansion of the second jet is considered, the flow areas of the left and right receivers can be described by Equation (1):

$$\begin{cases} A_{e1} = \left[ \frac{1}{2}(2b_{00} - l_m) + x_f + h \tan \alpha_2 \right] T_r (1 - \psi \lambda_j)^2 \\ A_{e2} = \left[ \frac{1}{2}(2b_{00} - l_m) - x_f + h \tan \alpha_2 \right] T_r (1 - \psi \lambda_j)^2 \\ A_{e3} = T_r l_r - A_{e1} \\ A_{e4} = T_r l_r - A_{e2} \end{cases} \quad (1)$$

In Equation (1)  $b_{00}$  represents the half-width of the second jet,  $l_m$  is the width of the shunt wedge,  $h_2$  is the distance between the deflector and the receivers,  $\alpha_2$  denotes the expansion angle of the outer boundary of the second jet,  $T_r$  is the thickness of the jet pan, and  $l_r$  is the width of the receiver.

### Jet velocity model for the left and right receivers

The existing momentum transfer models believe that the difference between the flow areas lead to inconsistent fluid flow into the two receiving chambers, resulting in different receiver recovery pressures.<sup>15,25</sup> However, numerical simulation of the flow field demonstrates that the velocity of the jet impinging on the left and right receivers also influences the recovery pressure, a fact which has never been considered before. Consequently, it is necessary to derive a jet velocity model for the left and right receivers.

It is normal to assume that the jet velocity for the left and right receivers is equal to the average velocity of the second jet. Because the average velocity of the second jet does not change with the motion of the deflector,<sup>25,26</sup> the jet velocity for the left and right receivers has been thought to be a fixed value. However, based on numerical simulation results, the actual velocity distribution of the second jet is not uniform due to the friction between the fluid and the wall. When the deflector moves, the jet velocities for the left and right receivers are inconsistent.

Figure 5 shows the velocity distribution curves for the second jet when the deflector is in the middle position (5(a)) and when it deviates to the right (5(b)). As illustrated in Figure 5, the  $x$ -axis represents the transverse

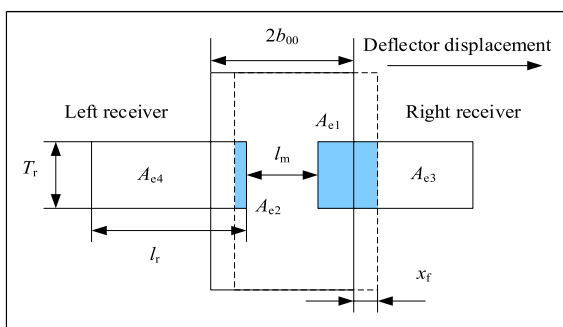


Figure 4. Flow areas of the left and right receivers.

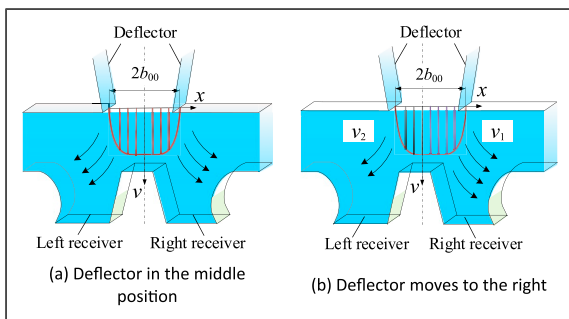


Figure 5. The actual velocity distribution curves for the second jet, (a) Deflector in the middle position, (b) Deflector moves to the right.

position of the second jet, the  $v$ -axis indicates the oil velocity, and the transverse position of zero indicates the symmetrical centerline of the left and right receivers.

For planar fluids, the line flow can be calculated using Equation (2):

$$f = u \times b \tag{2}$$

where  $f$  represents the line flow of the planar fluid,  $u$  is the average velocity of the planar fluid, and  $b$  is the width of the planar fluid.

Additionally, it is obvious that the line flows on the left and right sides should be equal while the deflector is in the middle position. On this basis, the jet velocities for the left and right receivers would be equal as well. However, the line flow on the right side increases and the flow on the left decreases as the deflector moves to the right, causing the jet velocities for the left and right receivers to no longer be equal. As shown in Figure 6, it was assumed that the line flows for the left and right sides when the deflector is in the middle position are both equal to  $f_1 + f_2$ , the average velocity of the right receiver jet is  $v_1$ , and the average velocity of the left receiver jet is  $v_2$ .

- (1) The deflector displacement is less than  $0.5b_{00}$

As shown in Figure 6, assuming that the increase in the line flow on the right is equal to  $f_3$ , the average velocities of the jet for the left and right receivers can be calculated using Equation (3):

$$\begin{cases} v_1 = \frac{f_1 + f_2 + f_3}{b_{00} + x_f} \\ v_2 = \frac{f_1 + f_2 - f_3}{b_{00} - x_f} \end{cases} \tag{3}$$

The maximum and average velocities of the second jet are denoted by  $u_{00m}$  and  $u_{01}$ , respectively. Based on the results of a flow field numerical simulation, there is a linear relationship between  $u_{00m}$  and  $u_{01}$ , as expressed by Equation (4):

$$u_{00m} = 1.15u_{01} \tag{4}$$

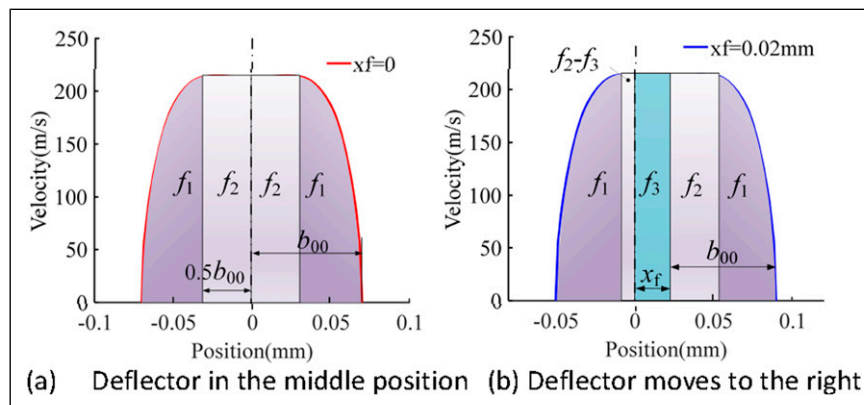
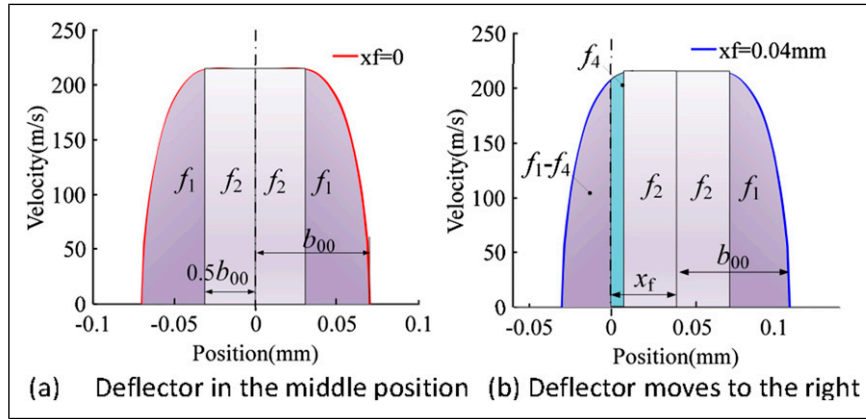


Figure 6. Velocity distributions for the second jet with (a)  $x_f = 0$  and (b)  $x_f < 0.5b_{00}$ .



**Figure 7.** Velocity distributions for the second jet with (a)  $x_f = 0$  and (b)  $x_f > 0.5b_{00}$ .

According to the definition of line flow, the line flows for the left and right sides ( $f_1, f_2, f_3$ ) can be expressed by Equations (5) to (7):

$$f_2 = 0.5u_{00m}b_{00} = 0.575u_{01}b_{00} \quad (5)$$

$$f_1 = u_{01}b_{00} - f_2 = 0.425u_{01}b_{00} \quad (6)$$

$$f_3 = u_{00m}x_f = 1.15u_{01}x_f \quad (7)$$

(2) The deflector displacement is greater than  $0.5b_{00}$

As illustrated in Figure 7, by assuming that the increase in the line flow on the right is equal to  $f_2 + f_4$ , the average velocities of the jet for the left and right receivers can be calculated using Equation (8):

$$\begin{cases} v_1 = \frac{2f_2 + f_1 + f_4}{b_{00} + x_f} \\ v_2 = \frac{f_1 - f_4}{b_{00} - x_f} \end{cases} \quad (8)$$

Based on the geometric relationship in Figure 7, the increase in the line flow ( $f_4$ ) can be approximately calculated using Equation (9):

$$f_4 = 1.15u_{01} \left( -\frac{1}{b_{00}}x_f^2 + 2x_f - \frac{3}{4}b_{00} \right) \quad (9)$$

### Recovery pressure model for the left and right receivers

As shown in Figure 8, the second jet impinges on the liquid in the receivers at speeds of  $v_1$  and  $v_2$ . According to the previously-stated hypothesis, the liquid in the receivers can be approximated as moving solid pistons with speeds related to the flow into the receivers.<sup>15</sup> Hence, it was assumed that the velocities of the moving pistons in the right and left receivers are  $v_{n1}$  and  $v_{n2}$ , respectively. At the same time, the reverse fluid formed by the impact of the second jet flows to the oil return port through the gaps at rates of  $v_{01}$  and  $v_{02}$ .

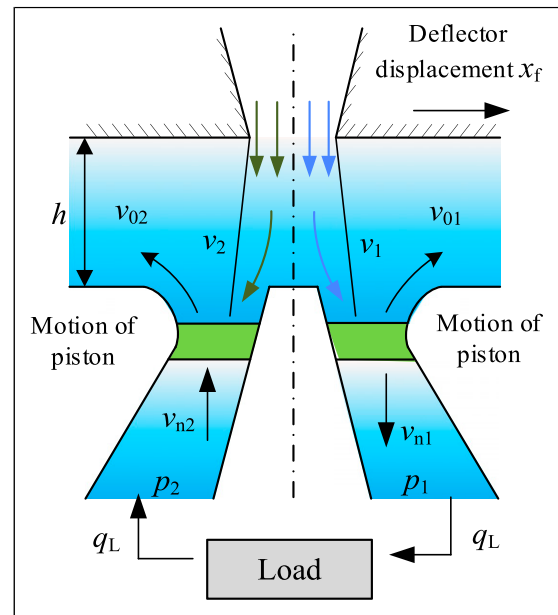


**Figure 8.** Recovery pressures for the left and right receivers.

Assuming that the fluid masses impinging on the moving pistons in the right and left receivers throughout time  $dt$  are  $dm_1$  and  $dm_2$ , respectively, they can be expressed by Equations (10) and (11):

$$dm_1 = \rho A_{e1}(v_1 - v_{n1})dt \quad (10)$$

$$dm_2 = \rho A_{e2}(v_2 + v_{n2})dt \quad (11)$$

The reverse fluid masses,  $dm_{01}$  and  $dm_{02}$ , reflected from the moving pistons throughout time  $dt$  can be expressed by Equations (12) and (13):

$$dm_{01} = \rho A_{e3}(v_{01} + v_{n1})dt \quad (12)$$

$$dm_{02} = \rho A_{e4}(v_{02} - v_{n2})dt \quad (13)$$

Therefore, according to the momentum theorem, the forces acting on the liquid in the left and right receivers can be calculated using Equations (14) and (15):

**Table 1.** Parameters and values of the deflector jet hydraulic amplifier.

Parameter	Symbol	Unit	Value
Inlet pressure	$p_s$	MPa	28, 21
Outlet pressure	$p_0$	MPa	0
Second jet average velocity (28 MPa)	$u_{01}$	m/s	211.23
Second jet average velocity (21 MPa)	$u_{01}$	m/s	182.93
Half-width of the second jet	$b_{00}$	mm	0.07
Shunt wedge width	$l_m$	mm	0.1
Receiver width	$l_r$	mm	0.4
Second jet height	$h$	mm	0.175
Jet pan thickness	$T_r$	mm	0.2
Receiver inclination	$\theta_2$	°	16.21
Expansion angle of the second jet <sup>25,26</sup>	$\alpha_2$	°	7
Jet type coefficient	$\psi$	/	0.04
Hydraulic oil density	$\rho$	kg/m <sup>3</sup>	839

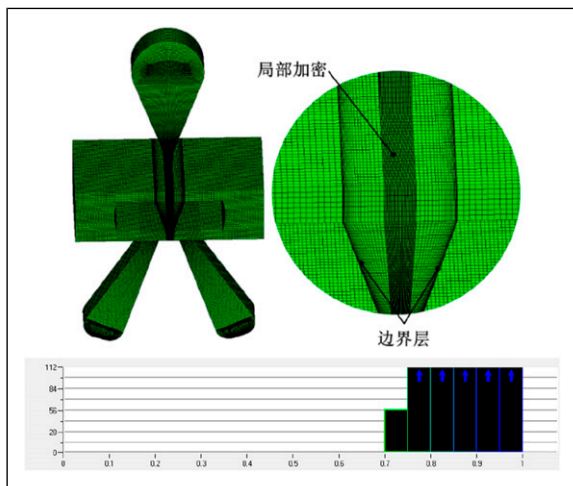


**Figure 9.** Mesh and mesh quality The specific information of cavitation model is as follows: vaporization pressure of oil is set to 4000 Pa; bubble radius is 0.001 mm; nucleation site volume fraction is 0.0005; evaporation coefficient is 50; condensation coefficient is 0.01.

$$R_1 = \frac{1}{dt} [dm_1 v_1 - (dm_1 - dm_{01}) v_{n1} + dm_{01} v_{01}] \quad (14)$$

$$R_2 = \frac{1}{dt} [dm_2 v_2 + (dm_2 - dm_{02}) v_{n2} + dm_{02} v_{02}] \quad (15)$$

By substituting Equations (10) to (13) into Equations (14) and (15) the impact forces,  $R_1$  and  $R_2$ , of the jet acting on the receivers can be computed using Equations (16) and (17):

$$R_1 = \rho A_{e1} (v_1 - v_{n1})^2 + \rho A_{e3} (v_{01} + v_{n1})^2 \quad (16)$$

$$R_2 = \rho A_{e2} (v_2 + v_{n2})^2 + \rho A_{e4} (v_{02} - v_{n2})^2 \quad (17)$$

If the flow through the receivers is given by  $q_L$ , then the velocities of the pistons and the reverse velocities of the fluid are given by Equations (18) to (20):

**Table 2.** Verification of iteration steps.

Iteration steps	Pressure of left receiver	Error(%)
10,400	4.006	
10,000	4.048	1.05
9600	4.112	1.58

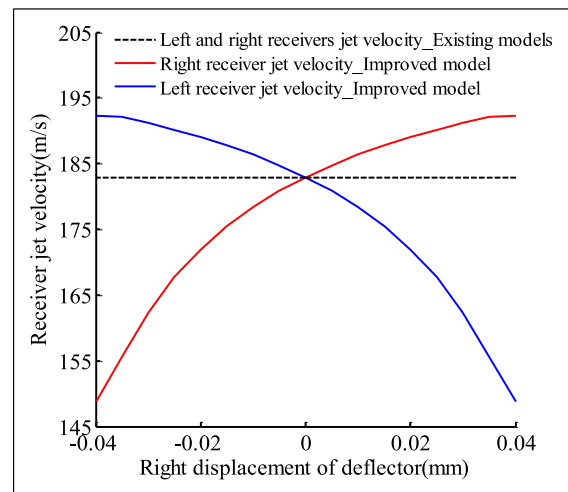


**Figure 10.** The differences in the receiver jet velocities between existing models and the improved model (21 MPa oil supply pressure).

$$v_{n1} = v_{n2} = \frac{q_L}{A_r} \quad (18)$$

$$v_{02} = \frac{v_2 A_{e2} + v_{n2} A_r}{A_{e4}} = \frac{v_2 A_{e2} + q_L}{A_{e4}} \quad (19)$$

$$v_{01} = \frac{v_1 A_{e1} - v_{n1} A_r}{A_{e3}} = \frac{v_1 A_{e1} - q_L}{A_{e3}} \quad (20)$$

Thus, the pressures,  $p_{10}$  and  $p_{20}$ , generated by the impact forces on the surfaces of the receivers can be calculated using Equations (21) and (22):

$$p_{10} = \frac{R_1}{A_r} = \rho \left[ \frac{A_{e1}}{A_r} (v_1 - v_{n1})^2 + \frac{A_{e3}}{A_r} (v_{01} + v_{n1})^2 \right] \quad (21)$$

$$p_{20} = \frac{R_2}{A_r} = \rho \left[ \frac{A_{e2}}{A_r} (v_2 + v_{n2})^2 + \frac{A_{e4}}{A_r} (v_{02} - v_{n2})^2 \right] \quad (22)$$

When oil enters a receiver, it acts on the end face of the slide valve to push the valve to move. Consequently, based on the Bernoulli equation, the recovery pressures,  $p_1$  and  $p_2$ , at the ends of the receivers can be described by Equations (23) and (24):

$$p_1 = p_{10} + \frac{1}{2} \rho q_L^2 \left( \frac{1}{A_r^2} - \frac{1}{A_{s1}^2} \right) \quad (23)$$

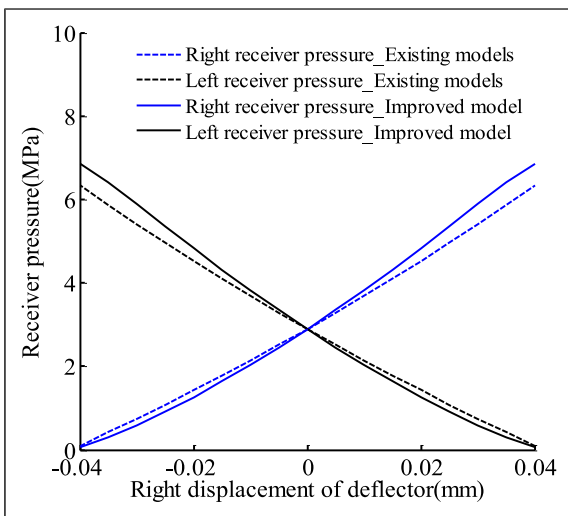


**Figure 11.** The differences in the receiver pressures between existing models and the improved model (21 MPa oil supply pressure).

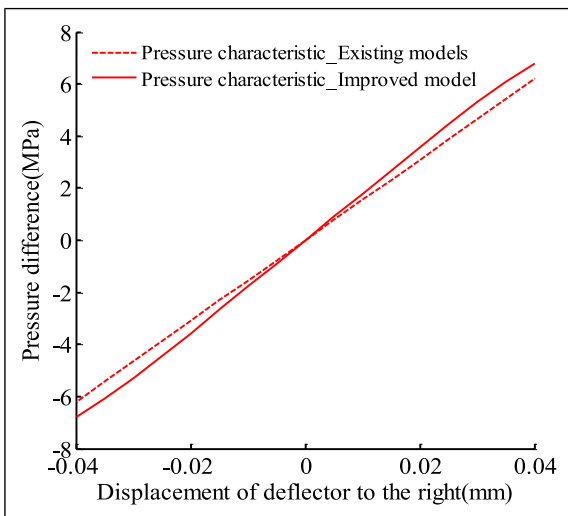


**Figure 12.** The differences in the pressure characteristics between existing models and the improved model (21 MPa oil supply pressure).

$$p_2 = p_{20} + \frac{1}{2} \rho q_L^2 \left( \frac{1}{A_r^2} - \frac{1}{A_{s2}^2} \right) \quad (24)$$

In Equations (23) and (24)  $\rho$  is the density of the oil,  $A_{s1}$  represents the area of the right end face of the valve, and  $A_{s2}$  represents the area of the left end face.

**Pressure–flow characteristics**

Due to the absorption effect in a turbulent submerged jet, the flow rate of a jet stream increases with increasing distance between the deflector and the receiving surface. If the displacement rate of the deflector is denoted by  $\gamma_f$  and defined as  $\gamma_f = |x_f|/b_{00}$ , then the flow increase rate,  $k_{aj}$ , caused by absorption is given by Equation (25):

$$k_{aj} = 0.45 - 0.33 \lambda_j \gamma_f - \lambda_j (0.35 \gamma_f)^2 \quad (25)$$

Equation (26) can be deduced from Equations (18) to (25):

$$p_L = p_1 - p_2 = \frac{\rho}{A_r} \left( A_{e1} \left( v_1 - \frac{q_L}{k_{aj} A_r} \right)^2 - A_{e2} \left( v_2 + \frac{q_L}{k_{aj} A_r} \right)^2 + A_{e3} \left[ \frac{A_{e1}}{A_{e3}} v_1 + \frac{q_L}{k_{aj}} \left( \frac{1}{A_r} - \frac{1}{A_{e3}} \right) \right]^2 - A_{e4} \left[ \frac{A_{e2}}{A_{e4}} v_2 + \frac{q_L}{k_{aj}} \left( \frac{1}{A_{e4}} - \frac{1}{A_r} \right) \right]^2 + \frac{1}{2} \rho \left( \frac{q_L}{k_{aj}} \right)^2 \left( \frac{1}{A_{s2}^2} - \frac{1}{A_{s1}^2} \right) \right) \quad (26)$$

where  $p_L$  represents the pressure difference between the left and right receivers,  $q_L$  is the flow through the receivers, and  $A_{e1}$ ,  $A_{e2}$ ,  $A_{e3}$ ,  $A_{e4}$ ,  $v_1$ , and  $v_2$  are all related to the deflector displacement,  $x_f$ . As a result, the pressure–flow characteristic equations for a deflector jet hydraulic amplifier are given by Equations (1), (3), (8) and (26).

**Pressure characteristic**

The pressure characteristic refers to the relationship between the load pressure and the deflector displacement under constant flow conditions. Generally, a constant load

**Table 3.** Errors in the pressure gain between existing models and the improved model.

Parameter	Improved model	Existing models	Error (%)
Pressure gain (MPa/0.01 mm)	1.78	1.55	12.92

is considered to be a blocking load, so it can be calculated by substituting  $q_L = 0$  into Equation (26):

$$p_L = \frac{\rho}{A_r} \left( A_{e1}v_1^2 + \frac{v_1^2 A_{e1}^2}{A_{e3}} - A_{e2}v_2^2 - \frac{v_2^2 A_{e2}^2}{A_{e4}} \right) \quad (27)$$

In Equation (27)  $p_L$  represents the pressure difference between the left and right receivers, and  $A_{e1}, A_{e2}, A_{e3}, A_{e4}, v_1,$  and  $v_2$  are all related to the deflector displacement,  $x_f$ . Therefore, the pressure characteristic equations for the deflector jet hydraulic amplifier can be obtained from Equations (1), (3), (8) and (27).

The pressure gain of the deflector jet amplifier at zero position can be expressed as (28):

$$K_{p0} = \left. \frac{\partial p_L}{\partial x_f} \right|_{x_f=0, q_L=0} = \frac{2\rho u_{m1}^2 l_r}{(l_r - b_{00} - h \tan \alpha_2 + l_m/2)^2 T_r} \quad (28)$$

### Flow characteristic

The flow characteristic refers to the relationship between the load flow and the deflector displacement when there is a constant load pressure. Substituting the load pressure  $p_L = 0$  into the Equation (26) the flow would satisfy equation (29):

$$\left[ \begin{aligned} &\left( \frac{1}{A_r A_{e3}} - \frac{1}{A_r A_{e4}} \right) + \frac{1}{2} \left( \frac{1}{A_{s2}^2} - \frac{1}{A_{s1}^2} \right) \\ &+ \frac{A_{e1} - A_{e2} + A_{e3} - A_{e4}}{A_r^3} \end{aligned} \right] \left( \frac{q_L}{k_{aj}} \right)^2 - \frac{2}{A_r} \left( \frac{A_{e1}v_1}{A_{e3}} + \frac{A_{e2}v_2}{A_{e4}} \right) \frac{q_L}{k_{aj}} + \left[ \begin{aligned} &\frac{A_{e1}v_1^2}{A_r} \left( 1 + \frac{A_{e1}}{A_{e3}} \right) \\ & - \frac{A_{e2}v_2^2}{A_r} \left( 1 + \frac{A_{e2}}{A_{e4}} \right) \end{aligned} \right] = 0 \quad (29)$$

Equation (29) is obtained by solving the equation for the load flow,  $q_L$ .

$$q_L = \frac{2k_{aj}A_{e1}A_{e4}v_1 + 2k_{aj}A_{e2}A_{e3}v_2 - 2k_{aj}A_{e3}A_{e4} \sqrt{\frac{(A_{e1}A_{e4}v_1 + A_{e2}A_{e3}v_2)^2}{A_{e3}^2 A_{e4}^2} - A_r \left( \frac{A_{e1} - A_{e2} + A_{e3} - A_{e4}}{A_r^3} + \frac{1}{A_r A_{e3}} \right) \left( -\frac{1}{A_r A_{e4}} + \frac{1}{2} \left( \frac{1}{A_{s2}^2} - \frac{1}{A_{s1}^2} \right) \right)}}{\left( A_{e1}v_1^2 + \frac{A_{e1}^2 v_1^2}{A_{e3}} - \frac{A_{e2}(A_{e2} + A_{e4})v_2^2}{A_{e4}} \right)} \quad (30)$$

$$2A_{e3}A_{e4}A_r \left( \frac{A_{e1} - A_{e2} + A_{e3} - A_{e4}}{A_r^3} + \frac{1}{A_r A_{e3}} - \frac{1}{A_r A_{e4}} + \frac{1}{2} \left( \frac{1}{A_{s2}^2} - \frac{1}{A_{s1}^2} \right) \right)$$

In equation (30),  $q_L$  represents the no-load flow through the receivers, and  $A_{e1}, A_{e2}, A_{e3}, A_{e4}, v_1,$  and  $v_2$  are all related to the deflector displacement,  $x_f$ . Therefore, the flow characteristic equations are given by Equations (1), (3), (8) and (30).

## Simulation

### Parameter values and simulation settings

The CFD software used in this manuscript is Fluent. Table 1 shows the related parameters and values of the deflector jet hydraulic amplifier. In addition, the average velocity of the second jet ( $u_{01}$ ) under different oil supply pressures was obtained by numerical simulation of the flow field.

The quality of mesh is checked with Determinant  $2 \times 2 \times 2$  as shown in Figure 9. The closer the Jacobian value is to 1, the better the grid quality is. It can be seen that the quality of the mesh checked by the Jacobian determinant is above 0.7, which proves that the mesh of the deflector jet amplifier has a good quality, laying a foundation for the subsequent finite element simulation. The wall y+ value is 1.8 at the wall of V-shaped slot.

The Iteration steps is set to 10,400, As we can see in Table 2, 10,400 steps are enough for a converged result.

### Simulation of differences between the improved model and existing models

To obtain an accurate analysis of the influence of the deflector motion on the receiver jet velocities, the

calculation results obtained from existing models and the improved model proposed in this paper are compared. As

a result, simulation curves for the receiver jet velocities and the deflector displacement were calculated by substituting the structural parameters into Equations (3) to (9) The calculation results are shown in Figure 10.

Figure 11 shows that existing models ignore the influence of the deflector motion on the receiver jet velocity, regarding it as a constant value. However, the simulation results show that when the deflector moves to the right, the jet velocity impinging on the right receiver increases and that on the left receiver decreases. The maximum error in the receiver jet velocity calculations between the improved model and existing models is 18.5%.

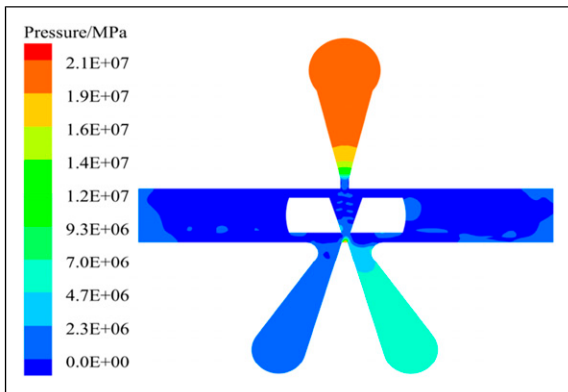


Figure 13. Pressure contour when the right deflector displacement was 0.02 mm (pressure characteristic).

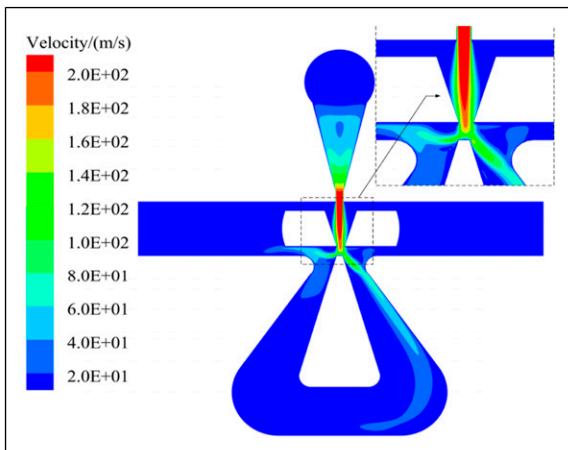


Figure 14. Velocity contour when the right deflector displacement was 0.02 mm (flow characteristic).

Furthermore, the difference between the receiver pressures obtained from the improved model and existing models was analyzed by substituting the structural parameters into the recovery pressure characteristic equations, Equations (23) and (24). These calculation results are shown in Figure 10.

Then, the structural parameters were substituted into the pressure characteristic equation, Equation (27) and the pressure characteristics of the improved model and existing models were obtained through calculations. The calculation results are shown in Figure 12.

Finally, to clearly compare the differences between the pressure characteristic calculation results for the improved model and existing models, the linear ratio of the pressure difference to the deflector displacement was defined as the pressure gain. The pressure gain results for the deflector jet hydraulic amplifier are shown in Table 3.

In summary, existing models ignore the influence of the deflector motion on the receiver jet velocities, which

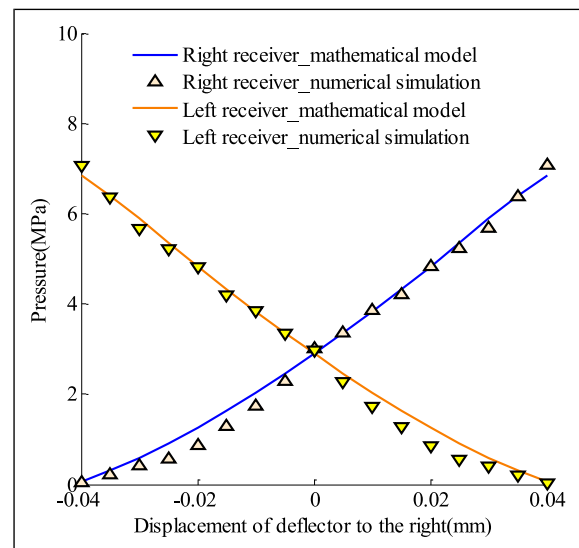
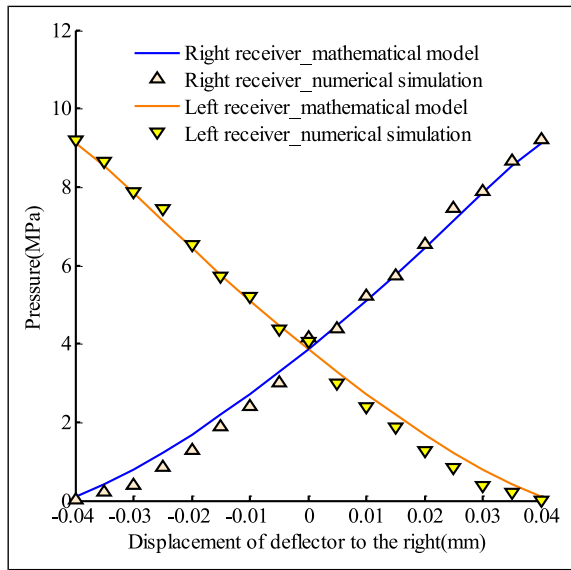


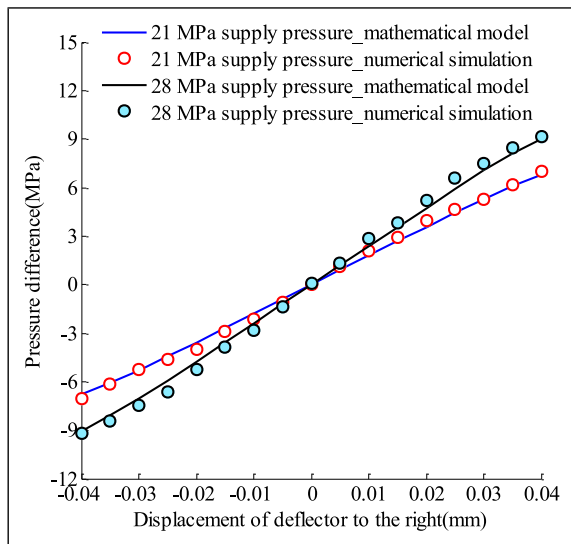
Figure 15. Pressure characteristic for the left and right receivers (21 MPa oil supply pressure).

Table 4. Receiver pressures and no-load flow (21 MPa).

Displacement, $x_f$ /mm	Pressure characteristics		Flow characteristics
	Left receiver pressure, $p_1$ /MPa	Right receiver pressure, $p_2$ /MPa	No-load flow, $q_L$ /(L/min)
0	3.02	2.97	0.000
0.005	3.37	2.28	0.031
0.01	3.85	1.74	0.051
0.015	4.20	1.29	0.072
0.02	4.83	0.86	0.089
0.025	5.21	0.37	0.106
0.03	5.67	0.22	0.119
0.035	6.38	0.11	0.121
0.04	7.07	0.04	0.123



**Figure 16.** Pressure characteristic for the left and right receivers (28 MPa oil supply pressure).



**Figure 17.** Pressure characteristic for the deflector jet hydraulic amplifier.

results in a 12.92% error when calculating the pressure gain of the deflector jet hydraulic amplifier.

**Simulation of the flow field**

To obtain a better description of the internal flow characteristics of the deflector jet hydraulic amplifier, a 3D flow field numerical model with a high quality mesh was built.

**Simulation settings.** The fluid in the deflector jet hydraulic amplifier flows with a complex turbulent motion involving a violent exchange of momentum and mass. For the flow field settings in the numerical simulations, a pressure-based solver and the RNG *k-ε* model were selected to obtain accurate pressure calculation results.

In addition, due to the inevitable cavitation phenomena that occur in the flow fields of high-velocity jets, mixing of the liquid and gas phases must be considered. Therefore, a mixture model was selected to obtain a more realistic description of the flow field. Here, the saturated vapor pressure of the oil was set to 4000 Pa and the oil viscosity at 40°C was 0.011,612 Pa·s.

**Flow field contour.** The experimental results demonstrate that the deflector displacement near the zero position was generally less than 0.04 mm. Hence, the left and right deflector displacements were selected as 0, 0.005 mm, 0.01 mm, 0.015 mm, 0.02 mm, 0.025 mm, 0.03 mm, 0.035 mm, and 0.04 mm.

As the deflector moved 0.02 mm to the right, the pressure contour for a typical section was extracted to observe the pressure distribution of the pressure characteristic flow field, as shown in Figure 13.

Observing the pressure contour shows that the fluid motion is a continuous process in which the pressure presents a variation trend of attenuation and then restoration. This transformation trend is consistent with the research concept in this paper of dividing different stages from top to bottom.

The velocity contour in the flow characteristic flow field for a 21 MPa oil supply pressure was extracted to

**Table 5.** Median pressure and pressure gain errors between the mathematical model and numerical simulation results.

Parameter	Supply pressure(MPa)	Mathematical model	Numerical simulation	Error(%)
Median pressure (MPa)	21	2.90	2.99	3.01
	28	3.86	4.09	5.62
Pressure gain (MPa/0.01 mm)	21	1.78	1.81	1.65
	28	2.32	2.45	5.31

observe the velocity distribution, as shown in Figure 14.

The velocity contour shows that the velocities of the second jet impinging on the left and right receivers are different when there is deflector motion. When the deflector moves to the right, the jet velocity for the right receiver increases and the jet velocity for the left receiver decreases. These flow field contour results verify the rationality of the improved model proposed in this paper and reveal the influence of the deflector motion on the receiver jet velocity.

### Comparison of the simulation results

To verify the accuracy of the improved model proposed in this paper, the flow field numerical simulation results are compared with the mathematical model results. Therefore, the recovery pressures in the receivers and the no-load flow were extracted from the results of the flow field numerical simulation, as shown in Table 4.

**Pressure characteristic.** First, the relationship between the receiver pressures and the deflector displacement was calculated by substituting the structural parameters into

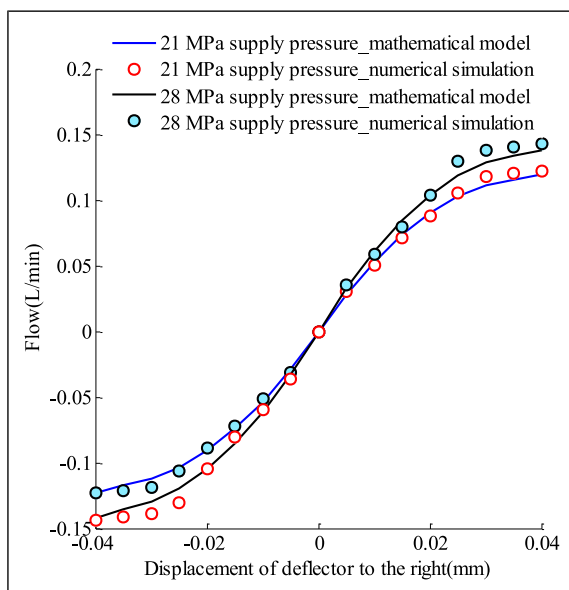


**Figure 18.** Flow characteristic for the deflector jet hydraulic amplifier.

the recovery pressure characteristic equations, Equations (23) and (24). The numerical simulation and mathematical calculation results are shown in Figures 15 and 16.

Then, the structural parameters were substituted into the pressure characteristic equation, Equation (27) and the pressure characteristic curve for the deflector jet hydraulic amplifier was obtained through calculations, as shown in Figure 17.

To calculate the error between the mathematical model and the numerical simulations, the receiver pressures at zero deflector displacement was defined as the median pressure, and the linear ratio of the receiver pressure difference to the deflector displacement was defined as the pressure gain. In that way, the error between the mathematical model and numerical simulation results were calculated, as shown in Table 5.

**Flow characteristic.** The no-load flow characteristic curve for the deflector jet amplifier was obtained by substituting the structural parameters into the flow characteristic equation, equation (29), as shown in Figure 18.

Similarly, to calculate the error between the mathematical model and the numerical simulations, the slope of the flow characteristic curve near the median of the deflector was defined as the flow gain. Table 6 shows the flow gain errors between the mathematical model and numerical simulation results for different oil supply pressures.

**Pressure–flow characteristic.** After computing the flow characteristic for the deflector jet hydraulic amplifier, the deflector displacement was selected as a fixed value and a series of  $q_L$  values were obtained. The load pressure,  $p_L$ , was calculated using the pressure–flow characteristic equation (26) and a cluster of pressure–flow characteristic curves were obtained, as shown in Figure 19.

The curves for the deflector jet hydraulic amplifier show that the pressure–flow characteristic has good linearity and symmetry near its zero position.

In summary, the pressure and flow characteristic for the deflector jet hydraulic amplifier were both predicted using the newly developed mathematical model and verified by numerical simulations. The verification results show that the maximum error between the mathematical model and numerical simulation results was 5.62%, which demonstrates that the theoretical model exhibits high calculation precision. Furthermore, the pressure and flow

**Table 6.** Flow gain errors between the mathematical model and numerical simulation results.

Parameter	Supply pressure(MPa)	Mathematical model	Numerical simulation	Error(%)
Flow gain ( $L \cdot \text{min}^{-1}/0.01 \text{ mm}$ )	21	0.054	0.053	1.89
	28	0.062	0.061	1.64

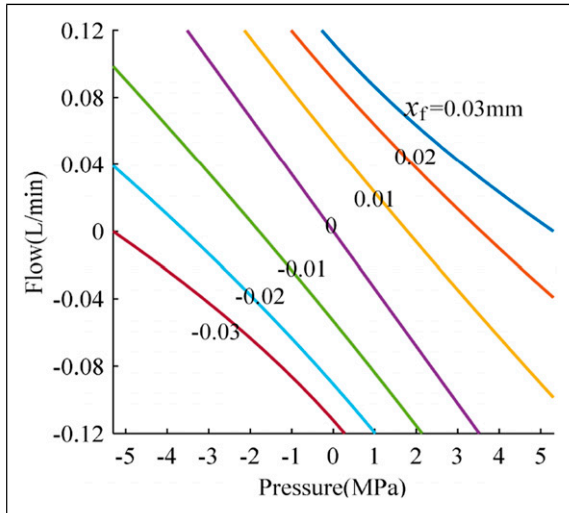


**Figure 19.** Pressure–flow characteristic for the deflector jet hydraulic amplifier.

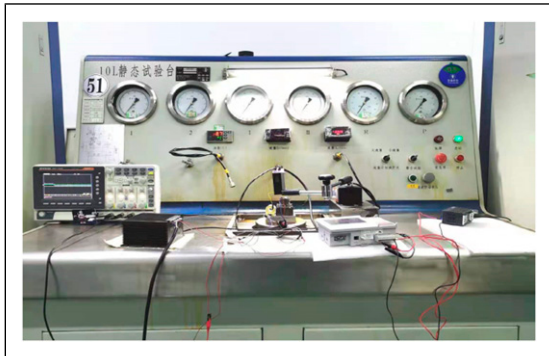


**Figure 20.** Experimental system.

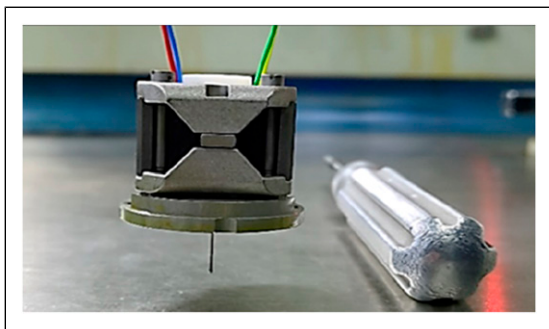


**Figure 21.** Tested deflector jet hydraulic amplifier assembly.

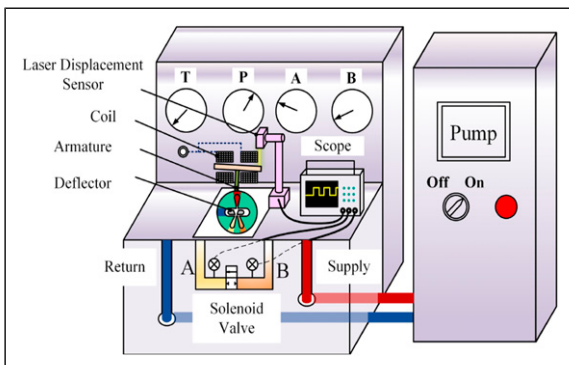


**Figure 22.** Schematic diagram of the experimental system.

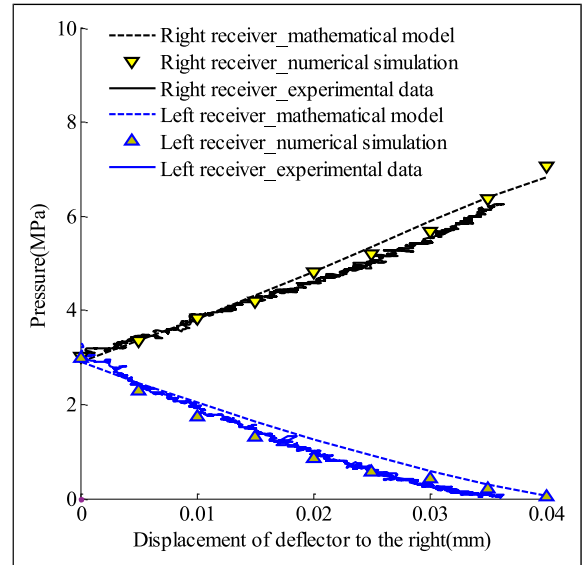


**Figure 23.** Pressure characteristics for the left and right receivers (21 MPa oil supply pressure).

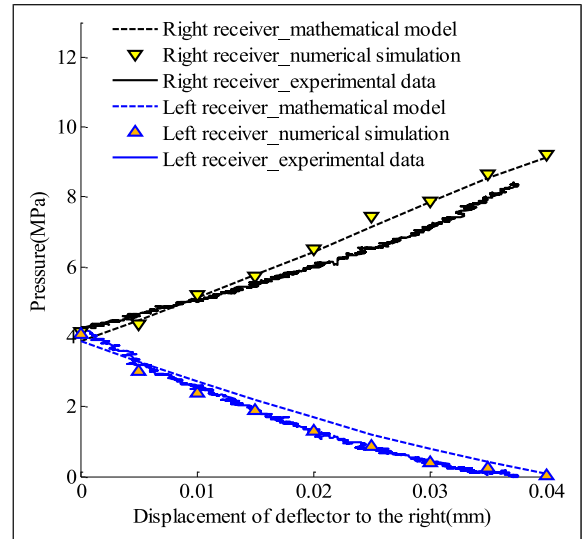


**Figure 24.** Pressure characteristics for the left and right receivers (28 MPa oil supply pressure).

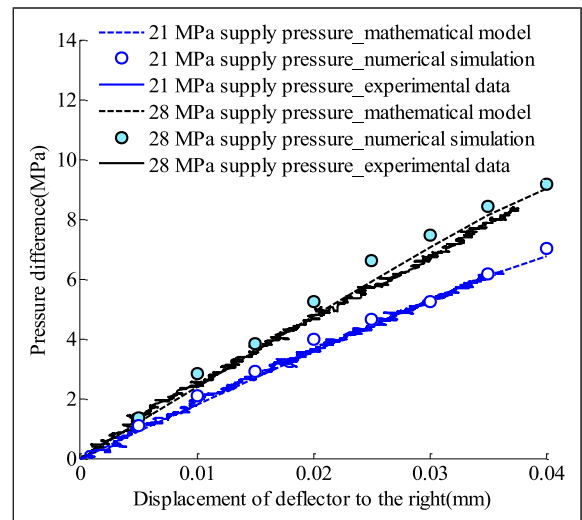


**Figure 25.** Pressure characteristic for the deflector jet hydraulic amplifier.

**Table 7.** Errors between the mathematical model and experimental data.

Parameter	Supply pressure (MPa)	Mathematical model	Experimental data	Error (%)
Median pressure (MPa)	21	2.90	3.06	5.23
	28	3.86	4.20	8.10
Pressure gain (MPa/0.01 mm)	21	1.78	1.74	2.30
	28	2.32	2.16	7.40

characteristic curves for the deflector jet hydraulic amplifier are similar to those for jet pipe hydraulic amplifiers, which is of great significance for further understanding the operation principles of the hydraulic amplifier.

## Experiment

To verify the accuracy of the mathematical model and the numerical simulations, an experimental research scheme was designed during this study to measure the pressure characteristic of the pilot stage.

### Composition and principle

The experimental system included a hydraulic pump, a hydraulic servo valve static test bench, a scope (GDS-1104B, frequency response  $\geq 20$  kHz), a pressure sensor (frequency response of 500 Hz, measuring precision of 0.01 MPa), a laser displacement sensor (CD530(A), measuring range of  $\pm 5$  mm, measuring precision of 0.2  $\mu\text{m}$ ), and the tested components (including a torque motor, an armature, and a deflector jet hydraulic amplifier). The experimental system and the tested deflector jet hydraulic amplifier assembly are shown in Figures 20 and 21, respectively.

As illustrated in Figure 22, the inlet of the deflector jet hydraulic amplifier was connected to an oil supply, the outlet was connected to an oil return, and the left and right receivers were connected to chambers A and B, respectively. The solenoid valve cut off the channel when testing the pressure characteristic. At first, a current pulse was sent through the coil, which drove the deflector to move around. At this time, the displacement of the armature was measured by the laser displacement sensor, and it was next transformed into the deflector displacement through the dimensional relationship. Finally, the pressures in chambers A and B were obtained by the pressure sensor, and the data were transmitted to the scope for display and recording.

### Experimental results

The experimental research regarding the deflector jet hydraulic amplifier was conducted for different oil supply pressures. After sorting the data, the pressure characteristic curves for the left and right receivers were obtained, as shown in Figures 23 and 24.

Moreover, the pressure characteristic curves for the deflector jet hydraulic amplifier are shown in Figure 25.

Similarly, the median pressure and pressure gain for the deflector jet hydraulic amplifier were selected to measure the error between the mathematical model and the

experimental data. These values were computed and are presented in Table 7.

It is speculated that the error may be caused by a machining error associated with the deflector jet hydraulic amplifier and limitations of the current jet theory for analyzing complex flow fields. The results demonstrate that the mathematical model is essentially consistent with the experimental data, which verifies the rationality of the flow field modeling method and the accuracy of the derived static characteristics equation.

## Conclusions

- (1) An improved model considering secondary jet velocity distribution for a deflector jet hydraulic amplifier that can predict the pressure and flow characteristics was developed. In this model, the jet velocity impinging on the receiving chambers is calculated, for the first time, to describe the effect of deflector motion on the second jet flow field. Through the study presented in this paper, it was found that the maximum error in the receiver jet velocity calculations between the improved model and existing models was 18.5%. Further studies conclusively showed that the maximum error in calculating the receiver recovery pressure between the improved model and existing models was 12%.
- (2) The mathematical model was verified by flow field numerical simulations and experiments. The maximum error between the mathematical model and numerical simulation results was 5.62%, and that between the mathematical model and experimental results was 8.10%. These error values demonstrate that the theoretical model for the deflector jet hydraulic amplifier exhibits a high calculation precision. This model fills the gaps in the theoretical research and lays a foundation for the structural design of deflector jet pressure servo valves.

### Declaration of conflicting interests

The author(s) declared no potential conflicts of interest with respect to the research, authorship, and/or publication of this article.

### Funding

The author(s) disclosed receipt of the following financial support for the research, authorship, and/or publication of this article: This study is supported by the National Natural Science Foundation of China (Grant No. 51975275), the Primary Research & Development Plan of Jiangsu Province (Grant No.

BE2021034), and Postgraduate Research & Practice Innovation Program of Nanjing University of Aeronautics and Astronautics (No. xcjxh20210502).

### ORCID iDs

Shenghong Ge  <https://orcid.org/0000-0002-2546-8887>

Hanhao Yang  <https://orcid.org/0000-0002-3934-3049>

Yuchuan Zhu  <https://orcid.org/0000-0002-7399-1656>

### References

1. Yin Q, Nie H, Wei X, et al. Aircraft electric anti-skid braking and combined direction control system using co-simulation and experimental methods. *Proceedings of the Institution of Mechanical Engineers, Part G: Journal of Aerospace Engineering*, 2020; 234(2): 173–191.
2. Liang T, Yin Q and Wei X. Straight-line path-following control for roll-out phase of the equipped-skid aircraft. In: *Proceedings of the institution of mechanical engineers Part G: journal of aerospace engineering*, 2022; 236(10): 2097–2107.
3. Tian YD. *Technology of electrohydraulic servovalves*. Beijing: Aviation Industry Press, 2008.
4. Wang CX. *Hydraulic control systems*. Beijing: China Machine Press, 2011.
5. Somashekhar SH, Singaperumal M and Kumar RK. Mathematical modelling and simulation of a jet pipe electrohydraulic flow control servo valve. *Proceedings of the Institution of Mechanical Engineers, Part I: Journal of Systems and Control Engineering* 2007; 221(3): 365–382.
6. Somashekhar SH, Singaperumal M and Kumar RK. Modelling the steady state analysis of a jet pipe electrohydraulic servo valve. *Proceedings of the Institution of Mechanical Engineers, Part I: Journal of Systems and Control Engineering* 2006; 220(2): 109–129.
7. Pham XHS and Yin YB. Research on fluid characteristics of jet pipe electro-hydraulic servo-valve based on structural parameters. In: *Intelligent Human-Machine Systems and Cybernetics*, Hangzhou, China, 24–25 August, 2024. 2012; 310–313.
8. Yin YB and Wang Y. Pressure characterization of the pre-stage of jet-pipe servo valve. *Journal of Aerospace Power* 2015; 30(12): 3058–3063.
9. Abdallah HK, Peng J and Li S. Analysis of pressure oscillation and structural parameters on the performance of deflector jet servo valve. *Alexandria Engineering Journal*. 2023(63): 675–692.
10. Saha BK, Peng J and Li S. Numerical and experimental investigations of cavitation phenomena inside the pilot stage of the deflector jet servo-valve. *IEEE Access*. 2020(8): 64238–64249.
11. Li J, Yan H, Ren YK, et al. Research on Flow Field in Pre-stage of Jet Deflector Servo Valve. *Acta Armamentarii* 2018; 39(5): 1012–1021.
12. Xing X. *Flow field modeling and structural parameter optimization of pre-stage of de-flector servo valve*. Wuhan, China: Wuhan university of science and technology, 2018.
13. Zhu YC and Li YS. Development of a deflector-jet electrohydraulic servovalve using a giant magnetostrictive material. *Smart Mater Struct* 2014; 23: 115001.
14. Li YS, Zhu YC and Wu HT. Parameter optimization of jet-pipe servovalve driven by giant magnetostrictive actuator. *Acta Aeronautica Astronautica Sinica* 2011; 32: 1336–1344.
15. Li YS. Mathematical modelling and characteristics of the pilot valve applied to a jet-pipe/deflector-jet servovalve. *Sensor Actuator A* 2016; 245: 150–159.
16. Li YS. Mathematical modeling and linearized analysis of the jet-pipe hydraulic amplifier applied to a servovalve. *Proceedings of the Institution of Mechanical Engineers*, 2019; 233(2): 657–666.
17. Wang CL, Ding F, Li QP, et al. Dynamic characteristics of electro-hydraulic position system controlled by jet-pan servovalve. *Journal of Chongqing University* 2003; 26(11): 11–15.
18. Kang S, Yan H, Li CC, et al. Modeling of the flow distribution and characteristics analysis of the pilot stage in a deflector jet servo valve. *Journal of Harbin Engineering University* 2017; 38(8): 1293–1302.
19. Yan H, Ren Y, Yao L, et al. Analysis of the internal characteristics of a deflector jet servo valve. *Chinese Journal of Mechanical Engineering*. 2019(32):1–13.
20. Saha BK, Li SJ and Lv XB. Analysis of pressure characteristics under laminar and turbulent flow states inside the pilot stage of a deflection flapper servo-valve: mathematical modeling with CFD study and experimental validation. *Chinese Journal of Aeronautics* . 2020 Mar 1;33(3): 1107–1118.
21. Mao QY, Yan H, Zuo ZQ, et al. Study on the formation mechanism of working pressure of deflecting jet servo valve. *Chinese Hydraulics & Pneumatics*. 2020(10):33–38.
22. Zhang XB, Ge SH, Zhou XZ, et al. Effect of asymmetry on null bias of deflector jet amplifier. *J Valve*. 2024(2): 154–161.
23. Yan H, Bai L, Kang S, et al. Theoretical model and characteristics analysis of deflector-jet servo valves pilot stage. *Journal of Vibroengineering* 2017; 19(6): 4655–4670.
24. Yan H, Wang FJ, Li CC, et al. Research on the jet characteristics of the deflector-jet mechanism of the servo valve. *Chinese Physics B* 2017; 26(4): 252–260.
25. Förthmann E. Über turbulente Strahlausbreitung. *Ing Arch* 1934; 5(1): 42–54.
26. Abramovich GN. The theory of turbulent jets. In: *Massachusetts*. Cambridge, Massachusetts: M.I.T. Press, 1963.